Available online at www.sciencedirect.com

ScienceDirect

Current Opinion in
Colloid & Interface Science

Finding the point of no return: Dynamical systems theory applied to the moving contact-line instability

J. S. Keeler[1,a] and J. E. Sprittles[2]

Abstract

The wetting and dewetting of solid surfaces is ubiquitous in physical systems across a range of length scales, and it is well known that there are maximum speeds at which these processes are stable. Past this maximum, flow transitions occur, with films deposited on solids (dewetting) and the outer fluid entrained into the advancing one (wetting). These new flow states may be desirable, or not, and significant research effort has focused on understanding when and how they occur. Up until recently, numerical simulations captured these transitions by focussing on steady calculations. This review concentrates on advances made in the computation of the time-dependent problem, utilising dynamical systems theory. Facilitated via a linear stability analysis, unstable solutions act as 'edge states', which form the 'point of no return' for which perturbations from stable flow cease decaying and, significantly, show the system can become unstable before the maximum speed is achieved.

Addresses

[1] School of Mathematics, University of East Anglia, Norwich, NR4 7TJ, UK

[2] Mathematics Institute, University of Warwick, Coventry, CV4 7AL, UK

Corresponding authors: Keeler, J.S. (j.keeler@uea.ac.uk); Sprittles, J. E. (j.e.sprittles@warwick.ac.uk)

[a] J.S.K gratefully acknowledges funding by the Leverhulme Trust, ECF-2021-017. J.E.S. gratefully acknowledges EPSRC under grants EP/W031426/1, EP/S022848/1 and EP/P031684/1 For the purpose of open access, the author has applied a CC BY public copyright licence to any Author Accepted Manuscript version arising from this submission.

Current Opinion in Colloid & Interface Science 2023, **67**:101724

This review comes from a themed issue on **Wetting and Spreading (2023)**

Edited by **Tatiana Gambaryan-Roisman** and **Victor Starov**

For a complete overview see the Issue and the Editorial

https://doi.org/10.1016/j.cocis.2023.101724

1359-0294/© 2023 The Author(s). Published by Elsevier Ltd. This is an open access article under the CC BY license (http://creativecommons.org/licenses/by/4.0/).

Keywords

Moving contact-line instability, Dynamic wetting, Dynamical systems.

Introduction

In this review article, we will overview recent advances in the understanding of the instability of a liquid–fluid interface traveling across a solid substrate; the so-called dynamic-wetting or moving contact-line problem. This flow forms the foundation of a broad array of industrial and natural processes, including in microfluidics [1], liquid-coating and printing operations [2], petroleum recovery [3], plant protection [4], groundwater hydrology [5], and biological processes [6], to name but a few.

Often, in applications, it is undesirable for the contact-line to become unstable—for example, in coating processes, it is well known that when the liquid–air–solid contact line moves too fast, air is entrained into the coating liquid as the system becomes unstable [8–10], and the quality of the coating film is poor. Therefore, understanding when and how these instabilities occur, and therefore how to prevent them, is an important practical problem that deserves scientific attention.

This article's primary aim is to discuss the aforementioned instability using a *dynamical systems* interpretation of the problem to offer fresh perspectives on a topic that has been the subject of multiple other review articles, e.g., recent ones including Afkhami, Gambaryan-Roisman, and Pismen [11]; Semenov, Starov, Velarde, and Rubio [12]; Andreotti and Snoeijer [13]; and Semenov, Starov, Velarde, and Rubio [14]. Various computational frameworks have been proposed to capture this class of flows, e.g., Volume-of-Fluid (VoF) [15,16], but the new approaches developed to analyse the instability are largely agnostic to these choices. This renewed emphasis on the dynamical systems approach emanates from a landmark study in Christodoulou and Scriven [17], which described how computational dynamical systems theory can be utilised in viscous flows with free-surfaces and also Severtson and Aidun [18], which examined two-layer flow in inclined channels using a normal-mode analysis. The renewed interest in using this framework stems from recent advancements in applying dynamical systems theory to complex fluid dynamics systems to help understand transition to instability phenomena, including classical turbulence in pipe flow [19], droplet breakup [20], and air bubble propagation [21,22]. Coupled with these are advances in computational efficiency and power, which make a wide range of problems accessible. Therefore, a new focus of these techniques on dynamic (de)wetting phenomena is timely.

Dynamical systems theory has a long and rich history, with contributions from leading scientific figures such

as Poincaré [23] and Kolmogorov [24], amongst others. The basic aim is to understand how the system evolves from an initial condition, and how certain objects, called *invariant objects*, can influence this transient journey (see, for example [25]). In the language of fluid dynamics, these invariant objects are typically *steady states*; flow configurations that don't change in time. However, other more exotic invariant objects can also exist, for example, time-periodic flow configurations, and probing the stability properties of these objects is a fundamental pursuit that the dynamical systems perspective allows. This theoretical framework, therefore, has immense potential in the context of the moving contact-line problem. Furthermore, whilst it is primarily viewed as a mathematical subject, recent developments in machine learning and concepts of 'big data', obtained from numerical simulations and/or experiments, have thrust dynamical systems' ideas into the limelight across a range of fields (see, for example [amongst many others], [26–28]) as finding the 'dominant modes' of a system containing sometimes millions of unknowns, or an experiment with noisy data, can now be found using increasingly sophisticated computational techniques, such as iterative eigensolvers [29], dynamic-mode-decomposition [30], and Koopman analysis [31]. This article will focus on how finding the 'dominant modes' of the dynamical wetting problem can be achieved by a linear stability analysis, using the corresponding eigenmodes.

The aims of this review are to illustrate the dynamical systems framework and methodology and to highlight a number of open questions and challenges that this methodology could help answer. We shall highlight a recent article that illustrates these ideas, Keeler et al. [7], while in §5, we shall give examples of experimental systems which could benefit from the dynamical systems framework reviewed here.

Instabilities in dynamic wetting

We now provide some detail of the instabilities present in (i) *dynamic-wetting*, where an *advancing* contact-line (ACL) 'wets' a solid as a liquid phase displaces a fluid (often air, though could be a second immiscible liquid but, for the sake of exposition, shall be referred to as the 'gas phase' in this article) and (ii) *dynamic-dewetting*, where a *receding* contact-line (RCL) 'dewets' a solid as the liquid phase retreats and is replaced by the gas phase, see Figure 1. In both cases, if the wetting speed is sufficiently small, a stable flow configuration is possible, but beyond a *critical (de-)wetting speed* the system becomes unstable; for example, in coating technologies, air entrainment occurs in the ACL and a growing thin-film is deposited on the solid in the RCL [7]. The principal aim of studies of this instability is to understand the physical conditions associated with this critical speed.

Figure 1

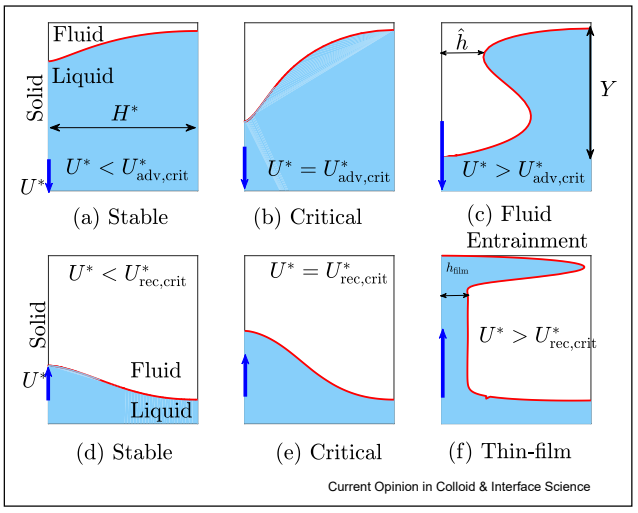

The upper row of panels shows the three regimes in an advancing contact-line problem, i.e., stable, critical, and air entrainment. The lower row of panels shows the receding contact-line problem, where a thin film develops instead. Taken from Keeler et al. [7].

In the ACL, the maximum speed of wetting occurs when a stable branch of solutions, as viewed in a suitable projection plane, e.g., by plotting a solution measure (for example, the length of the interface) against the substrate speed, joins an unstable branch of solutions (see Figure 4). This maximum speed of wetting can also be referred to as the *critical* speed of wetting, and both expressions shall be used in this article. This is a typical type of flow bifurcation in fluid dynamics denoted sometimes as a 'limit-point' bifurcation or as a 'fold' bifurcation (as it shall be referred to in this article). The speed at which the fold bifurcation occurs indicates the speed at which the system departs from steady flow and where air entrainment occurs, as visualised in a range of physical experiments, e.g., He [32]; Blake and Ruschak [33]; Simpkins and Kuck [34]; Duez, Ybert, Clanet, and Bocquet [35]; Pack, Kaneelil, Kim, and Sun [36]; and Vandre, Carvalho, and Kumar [37], by the emergence of a three-dimensional (3D) saw-tooth pattern, see Figure 2. In contrast, in the RCL the fold bifurcation indicates the emergence of thin-film formation [38,39]. These instabilities occur in a wide range of phenomena, for example, this instability is also visualised in droplets sliding down a substrate [40], but in what follows, we focus on coating-flow geometries where there is a moving substrate and unbounded fluid and gas phases. Interestingly, although fully-developed flow past the fold has intrinsic 3D structures [32,41], the critical value of the speed for the two-dimensional (2D) system often provides an excellent prediction to the onset of this behaviour (see, for example [42–44]); an observation which is yet to be fully understood. Three-dimensional perturbations, 'into the page' for the RCL

Figure 2

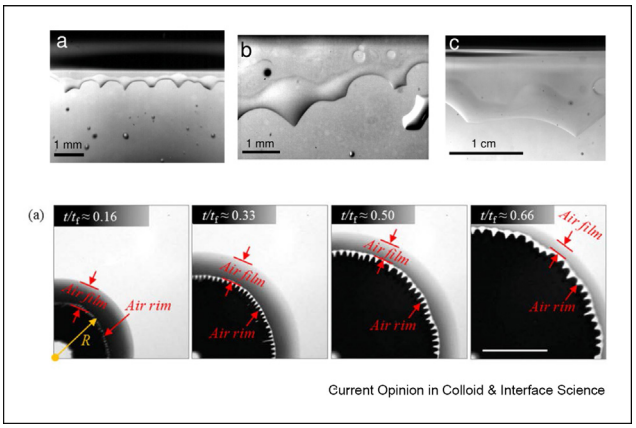

Top panel: Figure 7.14 taken reproduced with permission from Vandre [46] showing air entrainment (via bubbles emanating from the tips of the sawtooth 'vees') in the advancing contact-line in a coating-flow geometry. Bottom panel: Figure 2 adapted and reproduced with permission from Pack et al. [36] Copyright 2008 American Chemical Society. This experiment investigated the contact line instability caused by air rim formation under (nonsplashing) impacting droplets.

Figure 3

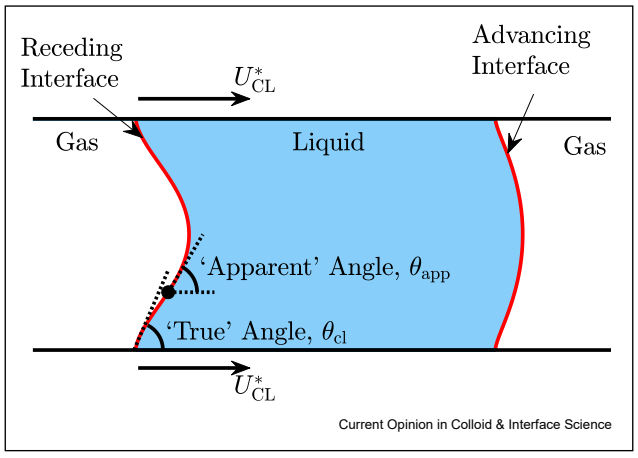

A liquid-bridge geometry, showing the difference between the apparent angle, measured a small finite difference away from the contact-point and the 'true' contact angle, θ_{cl}. Taken from Keeler et al. [59].

were investigated in [45] and for the ACL in Vandre [46], both using lubrication models and thus leaving plenty of scope for improvement in the ACL, where such models cannot accurately capture both phases; extensions will be discussed in section Open problems and new horizons.

Conventional modelling approaches

A range of different approaches have been proposed to describe the physics of the moving contact-line, but two of the most popular ways in which to describe the experimentally observed dynamics of the angle are (i) the *hydrodynamic theory* [47–49], based entirely on a macroscopic picture and (ii) the *Molecular-Kinetic theory* [50], in which the contact-line jumps across energy barriers in the substrate by thermally-activated molecular events [51,52]. One of the key differences that we highlight between these approaches is the treatment of the 'true' contact angle, θ_{cl}, see Figure 3. In (i) θ_{cl} is a constant, typically the equilibrium value which measures the wettability of the solid substrate. In (ii) however, θ_{cl} is determined using a formula that can relate the slip length, angle, and speed (see, recent articles [53]; [55]). It is still hotly debated which interpretation is correct, if both need to be combined, or whether more complex frameworks such as the interface formation model are required [56], but the arguments for and against will not be reviewed in this article as it has been the attention of numerous other review articles including Karim and Suszynski [57]; Afkhami et al. [11]; Semenov et al. [12]; Andreotti and Snoeijer [13]; and Bonn, Eggers, Indekeu, Meunier, and Rolley [58]. We shall take the simplest model, approach (i), and note that the techniques developed here can easily be applied to the other cases. Importantly, any 'viscous bending', leading to apparent dynamic angles, is resolved by our computations.

Often, modelling approaches are simplified by employing a lubrication (or 'thin film') approximation to the Navier–Stokes (NS) equations to allow a suite of analytic mathematical methods, for example, matched asymptotics, to be applied and to enable quantitative theoretical results and predictions can be made [38,45,48,49,60–67]. These analyses have provided invaluable insight, but they fail when (i) the contact angle is large and (ii) the viscosity of the upper fluid has to be taken into account as both fluids cannot be simultaneously 'thin'. The latter situation described is ubiquitous in the ACL problem, and thus the lubrication approximation is particularly poor in this case as observed in Vandre [46]. To avoid these parameter restrictions, the full NS equations have to be solved, which, historically, has been used as a 'last resort' due to the computational expense of calculation. However, due to the ever-advancing progress in scientific computing and numerical analysis (see, for example, [68,69]), these calculations have become increasingly more efficient, and calculating free-surface flows with the full NS equations is becoming less of a barrier [70,71]. Due to these advances, time-dependent solutions to the NS equations can be efficiently calculated in two dimensions (and also, albeit more expensively, in three dimensions) as long as the problem is not sufficiently multiscale, and this article will showcase these methods and results. In addition, as we shall show the linear stability algorithm, as described in Christodoulou and Scriven [17] and applied in Keeler et al. [7], is now far more tractable from a computational viewpoint due to the plethora of advanced linear algebra routines that can accurately and efficiently solve generalised eigenvalue problems (see, for example, [29,72]). Finally, the NS

Figure 4

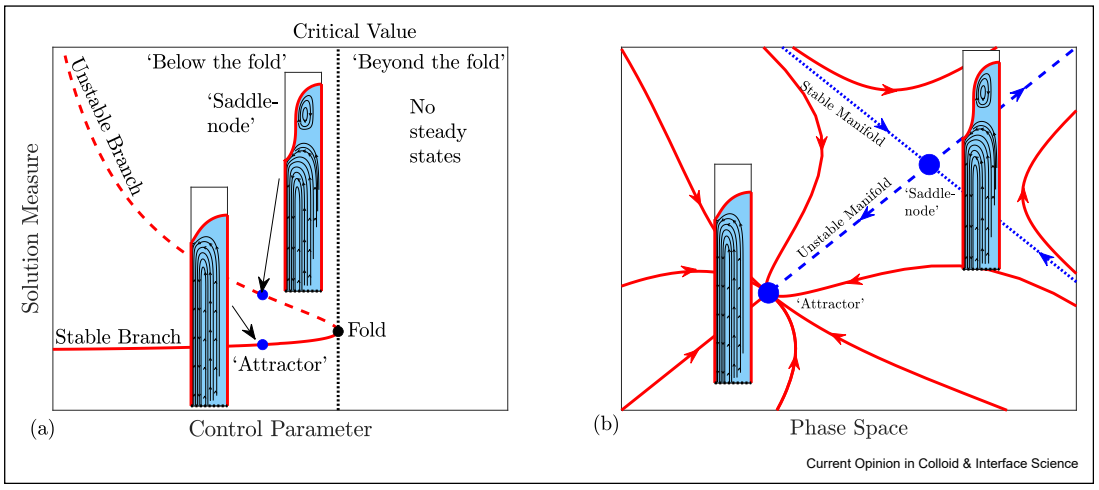

Panel (a): A fold-bifurcation solution structure. The horizontal axis represents a control parameter, and the vertical axis is a system measurement. As the control parameter is increased, two branches of steady states exist, meeting at a critical value of the control parameter called a fold bifurcation. Panel (b): A typical phase-plane sketch showing the stable 'attractor' and unstable 'saddle-node'. Lines with arrows represent trajectories that take the system from one state to another. The *stable* and *unstable manifolds* represent the boundaries of initial conditions that result in stable and unstable behaviour. Taken from Keeler et al. [59].

paradigm is often able to incorporate 'additional physics' as shall be discussed.

In the literature, for the hydrodynamic interpretation, which we henceforth focus on, there have been many studies that have calculated steady-state solutions (equilibria of the system) to the NS equations. Most of the original articles which uncovered and analysed the so-called 'moving contact-line problem', e.g., Huh and Scriven [73] and Dussan [74,75], focused on the steady case as did attempts to connect the actual and macroscopically observed (or 'apparent', see Figure 3) contact angles [48,76], where it was shown that three asymptotic regions exist, with, notably, an intermediate region where viscous bending of the interface occurs.

For the RCL, in a lubrication framework which assumes the outer phase is dynamically passive, a sequence of insightful articles, [60,61,77], showed that the inner region and outer regions can only be asymptotically matched when the speed of the solid, measured as a capillary number, $Ca = \mu U/\gamma$ (μ is the liquid's dynamic viscosity, U is speed of the substrate, γ is the surface tension), was less than a critical value, i.e., $Ca < Ca_{\text{crit}}$. In these papers, it was shown that the value of Ca_{crit} coincides with a fold bifurcation in the steady solution space, which is simply the location in parameter space where two branches of solutions meet (as seen in Figure 4; see Kuznetsov [25] for a detailed mathematical description of fold bifurcations in dynamical systems). In general dynamical systems, steady states on one branch (say the lower without loss of generality) are often stable and on the other (say upper) are unstable, although this is not always necessarily the case; they could both be unstable (although they could not be both stable). The stable and unstable branches of the RCL were then analysed using a lubrication model by Chan et al. [62]. However, this approach fails for the ACL, where if the outer fluid is assumed to be dynamically passive, a finite Ca_{crit} cannot be found.

More recently, the preceding analysis has been extended to general liquid–gas systems for lubrication models, where the gas phase has nonzero viscosity [65,78], free-surface cusp theory [64,79], and also for the NS model [43,46,80]. The addition of a dynamically active gas phase (nonzero pressure gradients) drastically alters the solution space for the ACL, and, similar to the RCL, a fold bifurcation then occurs at a finite Ca. Vandre et al. [80] showed that, physically, Ca_{crit} in the ACL occurs when the air-pressure gradient along the interface matches the strength of the capillary-stress gradient near the contact point. It was also demonstrated that the prediction of the value of Ca_{crit} for the ACL system is inaccurate when using the lubrication model as an approximation to the full NS equations[43,46,80]. The inclusion of additional physics, such as inertia, Marangoni flow, gravity, shear thinning/thickening, and thermal effects keep the fold-bifurcation solution structure intact [42,80]; [null]; [83–85] (these references will henceforth be attributed to the 'Minnesota group'). Another important development is that of the so-called *hybrid model*, where the liquid domain is modelled using the NS equations and the gas domain is accurately

modelled using lubrication theory (see [42,44,81–83, 86]). This has the added computational advantage that only approximately 50% of the domain has to be discretised, vastly reducing the computational demands, whilst still providing an excellent approximation to the full system.

Dynamical systems approach

Consider now how dynamical systems theory can be applied to this problem (and indeed any problem with fold bifurcations present). Central to dynamical systems theory is the investigation of the stability properties of fixed points, which, in fluid dynamics problems, are precisely steady states of the governing equation. There is a hierarchy of stability classifications that a steady state can possess. The strongest type of stability is *asymptotic* stability which implies that provided an initial condition is in the *basin boundary* of attraction, then the system will tend to the steady state as time tends to infinity. A weaker concept is *Lyapunov* stability that states if an initial condition lies sufficiently close to the steady state, then the system will remain in the vicinity of this steady state for all time. These definitions have no restrictions on the size of the initial deviation of the system away from the steady state and are often interpreted as *nonlinear* stability. *Linear stability* refers to asymptotic stability of the *linearised* equations; meaning that the results are only valid for sufficiently small perturbations away from the steady state. This is the most popular approach in fluid dynamics problems because the linearised system is far easier to deal with mathematically and to identify the stability properties (as discussed in the next paragraph). Also, small perturbations are often the most relevant class of perturbations for a given problem, especially if attempting to understand the response of the system to small amounts of noise, for example. Finally, we note that if a system is linearly unstable, then by definition it is also nonlinearly unstable, but the converse is not true; systems could be linearly stable but nonlinearly unstable. See Kuznetsov [25] and Holm, Marsden, Ratiu, and Weinstein [87] for a technical discussion of these ideas and some examples.

At a fold bifurcation, the steady state is no longer, what is termed, a *hyperbolic fixed point* of the system (not to be confused with a type of partial differential equation), which means that the *Jacobian* of the system at the steady state is singular. The Jacobian of the system is a matrix that describes the linear dynamics near to a solution, and thus, all of the (linear) stability properties are encoded in this matrix and, in particular, in the eigenvalues of the matrix [25,88]. Any eigenvalue with a positive real part represents *unstable modes* and any with a negative real part represents *stable modes*. At a fold bifurcation, an eigenvalue of the Jacobian crosses the imaginary axis (so that its real part changes sign), resulting in a switch of stability properties; indeed, a lot of the dynamics of the system can be summarised by solely looking at the behaviour of the system near a bifurcation point. The dynamical systems approach then proceeds in two stages. The first is to calculate families of steady states and utilise the information stored in the Jacobian matrix of the system in order to obtain their stability. The second step is to run simulations in time using the *eigenmodes* as initial conditions to see what effect the steady states (stable or unstable) have on the transient dynamics and eventual outcome of the system. The eigenmodes corresponding to the least stable eigenmodes can be thought as the 'dominant modes' in the dynamics near the steady state, but other algorithms, such as dynamic-mode-decomposition [30] and Koopman analysis [31], reveal 'dominant modes' of an entirely transient evolution of the system. However, often in experiments, the disturbance to the steady-state is not a 'clean eigenmode' and consists of experimental noise. One way to analyse this theoretically is to perturb the steady state by a linear combination of different eigenmodes and analyse the resulting time-dependent behaviour. It is possible for a disturbance consisting of a combination of entirely stable eigenmodes to become unstable through initial transient growth.[b] The amplification of small disturbances in this way is due to the non-normality of the eigenvectors which causes initial transient growth before nonlinearity can 'kick in' if the growth is sufficiently large. This has been explored in a number of fluid-dynamics problems (see, for example, [89–93]) and for the ACL problem (see Figure 13 in Keeler et al. [7]).

This approach has only recently been applied to (de-) wetting problems, where instead of focussing solely on the steady-state solutions of the NS equations, a 2D time-dependent computational framework was formulated to understand the effect of the stable/unstable states on the time-dependent evolution of the moving contact-line Keeler et al. [7]. The stability of the solution branches for both the RCL and ACL were probed using a linear stability analysis, and it was confirmed, as suspected, that one of the branches is unstable and the other stable. For values of $Ca > Ca_{\text{crit}}$, time-dependent simulations showed that for the RCL a thin film was deposited on the solid, whereas for the ACL, the second fluid was entrained along the solid 'into' the liquid, as expected. However, crucially, the system could also become unstable when $Ca < Ca_{\text{crit}}$ due to finite-amplitude perturbations of the steady-state (see, for example [94]), and the new theoretical framework allowed this effect to be fully explored. This work was extended to include a Molecular Kinetic theory–based description of the contact line in Keeler et al. [59] and showed excellent agreement with recent molecular dynamics simulations in Fernádez-Tolendano et al. [54].

[b] A simple example is this system of ODE's:$\dot{x} = -2\epsilon x + y, \dot{y} = -\epsilon y$, the eigenmodes are stable but initial conditions are possible for transient growth.

In this review, we will focus on time-dependent solutions of the NS system, leading to a detailed description of the dynamical systems approach to the moving contact-line problem. Fundamental to this is the existence of a fold bifurcation as the capillary number is increased. We will review what *minimal physical ingredients* are required in order for this fold bifurcation to be present. The dynamical systems interpretation is *independent* of the physics employed, and therefore, the authors believe it could be a useful new tool in the myriad of different physical models currently in the zeitgeist.

In §3, we will describe the common NS paradigm used in recent works, focussing on a list of basic assumption that produces the desired dynamics; in particular, we shall focus on the hybrid model that has great promise as an efficient scheme for this class of flows. In §A, we shall describe some features of the numerical models which may act as a guide for the reader when deciding how to implement their own moving contact-line code. In §4, we shall give a description of the recent new development of using a dynamical systems interpretation to the problem before discussing a number of open problems and challenges in §5.

Maximum speed of (de-) wetting

The aim of this section is to describe the main features of the governing equations which result in a maximum, or critical, speed of (de-) wetting and hence a fold bifurcation for the RCL/ACL problem. The equations are stated more thoroughly in Vandre [46]; Keeler et al. [7]; and Sprittles and Shikhmurzaev [95], and we refer the reader to these works (among others) for a full problem formulation of the NS equations.

Full hydrodynamic model

We demonstrate the model in the context of an idealised experiment: two-dimensional flow between two parallel plates, although other geometries have also been studied, including curtain-coating [42] and liquid bridges [59]. It is important to define a number of nondimensional parameters before proceeding; all dimensional quantities are denoted with stars. Quantities in the liquid, for example, the liquid in Figure 1, are denoted with a subscript 1, whilst the gas phase has subscripts 2. We define the viscosity ratio $\chi = \mu_2^*/\mu_1^*$, the Reynolds number, $\mathrm{Re} = \rho_1^* U^* H^*/\mu_1^*$, with reference to typical speeds U^* and length-scales H^*, density ρ_1^*, and the dimensionless slip length $\lambda = \lambda^*/H^*$. By assuming $\mathrm{Re} \ll 1$ and the Froude number $Fr = U^*/\sqrt{g^* H^*} \gg 1$ (where g^* is the gravitational constant), the dimensionless fluid ($i = 1$), and gas ($i = 2$) velocity and pressure $\mathbf{u}_i$ and p_i, respectively, satisfy Stokes flow equations in each phase:

$$0 = -\nabla p_i + \delta_i \nabla^2 \mathbf{u}_i, \qquad \nabla \cdot \mathbf{u}_i = 0, \qquad \delta_1 = 1, \delta_2 = \chi. \tag{1}$$

For a dynamically passive gas, assuming the surface tension coefficient γ^* of the liquid–fluid interface is constant, the dynamic and kinematic boundary conditions on the interface take the form

$$\boldsymbol{\tau}_2 \cdot \mathbf{n} - \boldsymbol{\tau}_1 \cdot \mathbf{n} = \frac{1}{Ca} \kappa \mathbf{n}, \qquad \frac{\partial \mathbf{r}}{\partial t} \cdot \mathbf{n} = \mathbf{u} \cdot \mathbf{n} \tag{2}$$

where $\boldsymbol{\tau}_i = -\mathrm{p}_i \mathbf{I} + \delta_i \left(\nabla \mathbf{u} + (\nabla \mathbf{u})^{\mathrm{T}}\right)$ is the dimensionless stress tensor of the liquid and the gas, κ is the curvature of the interface, $\mathbf{n}$ is the outward normal vector (pointing towards the fluid phase) of the interface, and $\mathbf{r} = (x_s, y_s)$ is the unknown position of the interface. On the walls, we have a no-penetration condition and employ a Navier-slip model i.e.,

$$\lambda(\boldsymbol{\tau}_i \cdot \mathbf{n}) \cdot \mathbf{t} = (\mathbf{u}_i - \mathbf{U}) \cdot \mathbf{t}, \qquad \mathbf{u}_i \cdot \mathbf{n} = 0, \tag{3}$$

where $\mathbf{n}$, $\mathbf{t}$ are the vectors normal/tangential to the substrate, respectively, and $\mathbf{U} = (0, \pm U)$ on the moving wall and $\mathbf{U} = \mathbf{0}$ on other walls, and appropriate far-field conditions are applied on the inflow/outflow boundaries. Finally, we assume the contact angle is constant. For the ACL we have to take into account the fluid velocities and pressures in *both* phases as the air's 'strength' is increased when it forms thin layers near the contact line. In contrast, for the RCL problem, as shown in Vandre et al. [80] and Keeler et al. [7], air as an outer phase is typically passive, and, provided the contact angle is smaller than 90°, a lubrication approximation often works well (see [60–62,77]).

Notably, the presence of gravity does not significantly change the value of Ca_{crit}, but as the branch is traversed upwards, extra 'wiggles' in the curve occur, corresponding to extra oscillations on the interface, see Chan et al. [62] and bottom panel of Figure 8.

Finally, we note these are the *minimal physical ingredients* required to ensure that a critical capillary occuring in both the RCL and ACL exists. The Minnesota group has included numerous additional physics in their NS models, but all share the common feature that a fold bifurcation is observed in the solution structure.

Hybrid model

For the ACL, the velocities and pressures in the upper gas phase have to be resolved. However, the computational cost of a two-layer problem can be drastically reduced by implementing a thin-film approximation in the phases for which it is valid [49,66,67], which leads to a hybrid model (see [42,81–84,86]) that approximately halves the number of unknowns in the problem and avoids meshing very small elements in the outer phase as variables in the upper gas phase are only computed on the interface between the gas and liquid. An additional assumption this model makes is that the ratio $\widehat{h}/Y \ll 1$ (see Figure 1), resulting in the flow

becoming approximately parallel to the substrate. Then, instead of solving Stokes flow in the gas phase, a lubrication model is applied to determine the pressure on the interface. Mathematically, one solves a surface Partial Differential Equation (PDE) for the pressure in the gas phase only, along the interface, which can then be coupled to liquid phase via the boundary conditions (see Keeler et al. [7]; Vandre [46]; Liu et al. [82] for details), namely we solve

$$\frac{\partial \mathbf{r}}{\partial t}\cdot\mathbf{n} \pm \frac{1}{\chi}\frac{\partial Q_2}{\partial s} = 0, \qquad Q_2 = \frac{1}{6}\frac{\partial p_2}{\partial s}h^3 + \frac{1}{2}Ah^2 + Bh \quad (4)$$

where s is the arclength along the interface measured from the contact point, p_2 is the dimensionless pressure of the gas along the interface, the $\pm$ sign indicates the ACL/RCL problems, respectively, h is the perpendicular distance of the interface from the moving solid, and A and B are functions of the system parameters (see Keeler et al. [7] for a detailed description).

There has been extensive validation of the hybrid model for the steady ACL against the full system and experiment [42,82] and for the time-dependent hybrid model [7]. Here, we do not use the hybrid model for the RCL as the outer phase is considered dynamically passive anyway.

As shown in a large number of research articles [42, 45, 59, 61, 64, 77, 81, 82, 82–84, 86], steady solution curves can be traced extensively for a wide range of physical parameters, and the solution structure broadly looks like that in Figure 5. The main difficulties in computing the lower and upper bifurcation curves are that (i) as the fold bifurcation is approached, pressure gradients can become large [80,83] so that the mesh needs to be sufficiently resolved around the contact line and (ii) as the upper branch is traced, the interface becomes multivalued [7,62], i.e., the interface develops a stationary inflection point, see panels A3 and R3 in Figure 5. The first difficulty is overcome by mesh refinement, and the second difficulty can be resolved by choosing to parameterise the interface as a function of the arc length, i.e., $\mathbf{r} = (x_s(s), y_s(s))$. See appendix A for a discussion of these points.

Edge states of the moving contact-line problem

Now that the physical conditions for a maximum speed of (de-)wetting and the existence of a fold bifurcation have been established, we discuss recent progress by Keeler et al. [7] in applying dynamical systems theory to the moving contact-line problem. Whilst the approaches outlined in the previous section focus on steady flow, in Keeler et al. [7,59], the time-dependent stability properties of the steady states were probed systematically. We note that this is not the first time these ideas have been used in this class of flows, for example, Chan et al. [62] used bifurcation theory to approximate the unstable branch near the fold bifurcation using a lubrication model. However, the chief novelty of Keeler et al. [7] is the implementation of a full hydrodynamical model that captures the RCL and ACL as subsets of the same problem; thus, treating them within a single theoretical and computational framework. This work was in the same spirit as the study by Christodoulou and Scriven [17] who numerically calculated the eigenmodes of a free-surface coating flow and also Severtson and Aidun [18] who calculated normal modes of a viscous two-layer shear flow.

The approach considered is inspired by ideas from dynamical systems theory (see, for example, [25]) which have successfully been applied to a number of other different fluid dynamics problems. In this interpretation, the governing equations can be written in the form

$$R(\dot{\mathbf{w}}, \mathbf{w}) = 0, \quad (5)$$

where the vector $\mathbf{w}$ represents all of the unknowns in the problem, (i.e., $\mathbf{w} = [\mathbf{u}, p, \mathbf{r}]$ in this problem), R is a nonlinear operator, and $\dot{\mathbf{w}}$ represent time derivatives in the system. We again emphasise that equation (5) is a completely general representation of a physical system and, e.g., is independent of the physics chosen for a particular dynamic wetting model.

The geometric interpretation of this system is that steady states (and other *invariant objects*) of the governing equations are located in a finite space of the infinite-dimensional phase space of the system, see Figure 6. A given initial condition will result in a trajectory through this phase space and can potentially interact with the collection of invariant objects which will alter its final dynamical outcome; steady states could be stable and act as an 'attractor' to the system or so-called 'edge-states', weakly unstable invariant objects, could act subtly, 'directing' trajectories to different dynamical outcomes. These ideas are shown in the top panel of Figure 6 where the phase space is shown as a 2D projection in a plane parameterised by two solution measures; these could be, for example, the length of the interface, i.e., $L = \int \mathrm{d}s$, where the integral is over the interface, and s is the arclength, and the height of the interface, i.e., $\mathrm{Y} = \mathrm{y}(1) - \mathrm{y}(0)$ see Figure 1. Therefore, the calculation of these objects, and hence revealing their location in parameter space, is crucial in understanding the eventual dynamical outcome of the system.

This interpretation is pertinent to the moving-contact-line problem because of the existence of the fold bifurcation at the critical capillary number and the existence of an upper branch of solutions, which have always been viewed as being unstable but never explicitly investigated. The methodology described can now be used to determine *quantitative* stability

properties. Furthermore, by explicitly calculating the unstable branch of solutions by slightly perturbing these unstable states (impossible to do in a physical experiment), the influence of these states on the overall dynamics of the system can be found. In Keeler et al. [7], these dynamical systems ideas were deployed to address the following three questions:

(Q1) : Is the upper branch of solutions unstable as suspected but never shown mathematically?
(Q2) : What effect does this upper branch of solutions have on the dynamics of the system; if any, when $Ca < Ca_{\text{crit}}$?
(Q3) : What happens when $Ca > Ca_{\text{crit}}$?

Figure 5

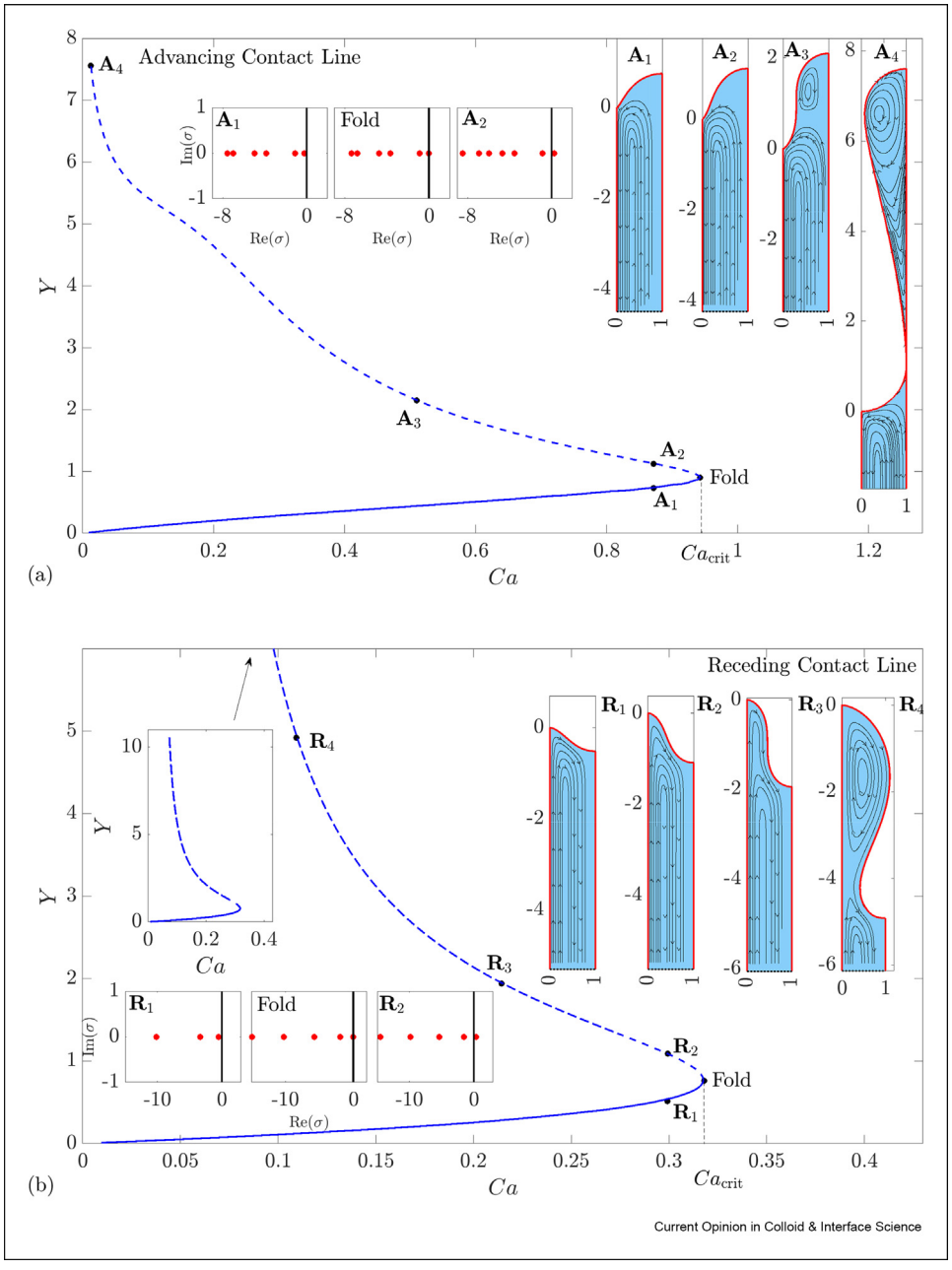

The bifurcation structures of (**a**): advancing contact-line problem and (**b**): receding contact-line problem. The solid/dashed lines indicate stable/unstable solutions, respectively. The vertical measure is the height of the interface, *Y*, as shown in figure 1. Inset figures are interface profiles with streamlines indicated by markers on the solution curve in the main panel. The eigenspectra are also displayed as red markers in the inset diagrams. Taken from Keeler et al. [7].

To answer (Q1), a steady state, denoted by $\mathbf{w}_\star$, is perturbed by an eigenmode which has a spatial dependence $\mathbf{g}$ and a time dependent exponential, e^{st}, i.e., we insert

$$\mathbf{w} = \mathbf{w}_\star + \epsilon \mathbf{g} e^{st} \tag{6}$$

into (5), where ϵ is a small parameter. We emphasise that we are not assuming normal modes and that $\mathbf{g}$ is unknown *a priori*. At leading order, (in ϵ) the equations in (5) are simply the equations for the steady state, but at the next order, the linearisation procedure results in a generalised eigenvalue problem stated as

$$s\mathbf{M}(\mathbf{w}_\star)\mathbf{g} + \mathbf{J}(\mathbf{w}_\star)\mathbf{g} = 0 \tag{7}$$

that has to be solved for the spectrum of eigenvalues s, corresponding to growth rates and corresponding eigenmodes $\mathbf{g}$, where $\mathbf{M}(\mathbf{w}_\star)$ and $\mathbf{J}(\mathbf{w}_\star)$ are the mass-matrix and Jacobian-matrix evaluated at the steady state $\mathbf{w}_\star$, respectively. If Real$(s)<0$, then the steady state is linearly stable as all perturbations decay, if Real$(s) > 0$, the steady state is unstable as perturbations grow, and if Real$(s) = 0$, then a bifurcation has been located as discussed earlier. This approach, as implemented in Keeler et al. [7], demonstrated that the lower branch is stable and the upper branch is unstable by calculating the values of s as the steady-state solution branch was traced out, thus answering (Q1); the results are shown in Figure 5.

The computed eigenmodes, $\mathbf{g}$, from this stability analysis also helped answer (Q2). An initial condition for the system can be composed of the steady state plus a linear combination of these eigenmodes. This is a convenient way of perturbing the interface that allows all of the boundary conditions to be satisfied as the form of the perturbation satisfies these conditions by design. The eigenmode associated with the most unstable eigenmode effectively 'stretches' the interface of the steady state in the vertical direction, whilst other eigenmodes create 'wobbles' on the interface. Thus, an initial condition based on a linear combination of these eigenmodes can represent physical perturbations to the system, if known, or could be considered as a crude approximation to 'noise' in the system.

By solving the time-dependent model for $Ca < Ca_{\text{crit}}$, it was found that sufficiently small 'stretch' perturbations return to the steady state, and the unstable state on the upper branch (at the same capillary number) acts as the 'point of no return'; if the stable state gets perturbed beyond this, then the system becomes transient and air entrainment/thin-film development occurs. The unstable state on the upper branch is thus an 'edge state', a state that separates trajectories that return to the steady state from those which will evolve transiently for all time. The main consequence of this is that the system can become unstable if $Ca < Ca_{\text{crit}}$ due to finite-amplitude perturbations from the steady state. This is significant as the identification of Ca_{crit} in experiments is based on when the system becomes unstable; if this occurs before the actual critical point, then the experiment is only identifying a lower bound for the critical value. The concepts of 'edge states' have been used extensively in the transition to turbulence problem [19] and other fluid dynamics problems (see, for example, [20,21]), but the identification of an 'edge state' in this system is novel and has the potential to open up new avenues of research in this problem. For example, an interesting feature of 'edge states' is that the system can 'walk the tightrope' by staying in the vicinity of the 'edge state' for an arbitrarily long time before it will eventually leave the influence, see Figure 6.

Finally (Q3) can be answered by solving an Initial Value Problem (IVP), for example, for simplicity, with the interface initially flat and the fluids initially at rest.

Figure 6

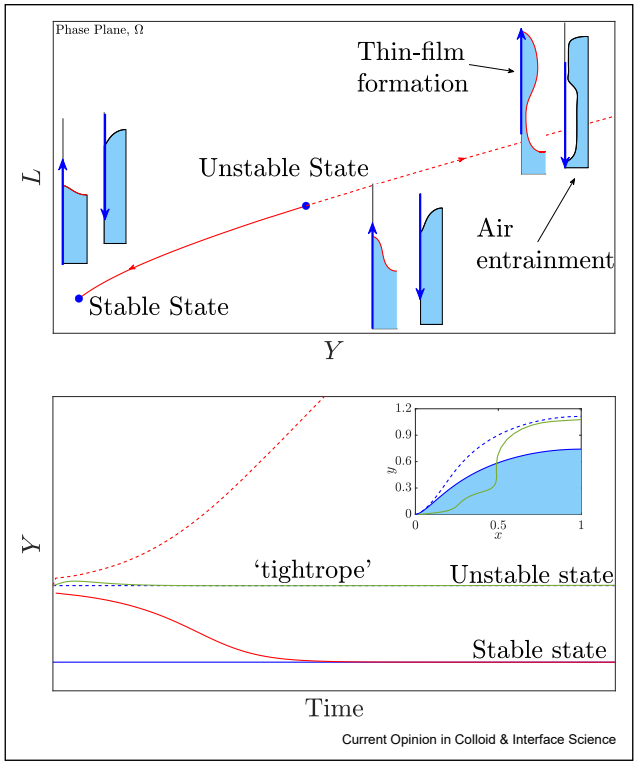

Top panel: Phase-space sketch for the advancing contact-line and receding contact-line in the (Y, L) plane. The stable and unstable states are denoted as circular markers. The red arrowed lines indicate trajectories that eventually relax to the stable state (solid line) and those that become unstable (dashed line). The thick blue arrows in the inset figures indicate the direction of motion of the moving substrate. Bottom panel: The time plot of three trajectories that become stable (solid red line), unstable (dashed red line), and one that 'walks the tightrope' and stays in the vicinity of the 'edge' state for an arbitrary amount of time (solid green line) are shown. The inset diagram shows the initial condition (in green) of the trajectory that 'walks the tightrope' with the stable (solid blue) and unstable (dashed blue) states also plotted.

Keeler et al. [7] were unable to find any other solution branches in this parameter regime, and the calculations based on the hybrid method showed how air entrainment and thin-film development occurs, see Figure 4. This does not discount the existence of other solution branches; it just confirms that starting from rest, a different steady state is not reached; other initial conditions which are not at rest may evolve to a different steady state, although there is no evidence for the existence of such a state.

In Keeler et al. [7], the answers to (Q1)−(Q3) were verified for the ACL and RCL, and the qualitative behaviour of the stability of each system was identical (notwithstanding the fact that ACL develops into air entrainment, and the RCL develops into a thin film). A follow-up paper [59] concentrated on the RCL in a liquid-bridge geometry and explored the thin-film development further by using the theory of Landau and Levich [96], but in principle, the stability algorithm of Keeler et al. [7] can be applied to include any additional physics or domain geometry and has the potential to be applied to an untold number of different problems.

One obvious extension to the work of Keeler et al. [7,59] is to introduce inertia. Steady solutions with inertia have been calculated before [80], but the dynamics of the system will be expected to be more complex than the Stokes-flow scenario investigated in Keeler et al. [7]. Although it was shown in Vandre et al. [80] that inertia does not change the qualitative structure of the fold-bifurcation solution structure, it is not unreasonable to suggest, based on the transition to turbulence problem, that more exotic invariant objects, such as periodic orbits and heteroclinic orbits (trajectories in phase space that connect different steady states), may populate phase space and have subtle yet important effects on the dynamics.

Finally, we note that it is convenient to measure the apparent angle, θ_{app} as the angle the interface makes to the vertical at the inflection point (i.e., when $\kappa = 0$). We emphasise that the fold bifurcation does not in general coincide with where $\theta_{\text{app}} = 0$ as shown in panels A1−A3 and R1−R3 of Figure 5, which show that θ_{app} first vanishes on the upper branch, past the fold bifurcation. This result has been reported before by the Minnesota group (see Figure 6 of [80]) for the ACL and by Keeler et al. [7,59] for the RCL, yet it is not uncommon for the critical *Ca* to be estimated in experimental studies using the fact that $\theta_{\text{app}} = 0$. This is true, mathematically, in the asymptotic limit as the (dimensionless) slip length tends to zero as demonstrated in Eggers [61,77] and others. In other geometries, particularly on the nanoscale, the slip length can be comparable to the domain size, and hence, we would not expect the onset of instability to coincide with the location in parameter space where the interface develops an inflection point. We also note that this has been seen in recent experiments where an interface angle of around 10° is observed near the critical capillary number [97].

Open problems and new horizons

We now highlight three physical systems where computationally efficient numerics combined with a dynamical systems approach could help resolve some experimentally discovered open problems.

Thick-film formation

For plate withdrawal geometry (RCL), Snoeijer et al. [39] predicted that in addition to a Landau−Levich thin film, another thicker film could also develop. More recently, as shown in their PhD thesis and a recent article by Hayoun [98] and Hayoun, Letailleur, Teisseire, Lequeux, Verneuil, and Barthe [99], these thick-film solutions were also identified using techniques shown in Figure 7 in experiments and theoretically using a lubrication model. Due to the development of the RCL time-dependent model in Keeler et al. [59], the calculation of these steady states and a corresponding stability analysis could identify how the thick film develops and whether unstable states guide the system to the formation of a thick film. As shown in Keeler et al. [59], a thick-film solution is not produced when solving a purely pressure-driven flow, so there must be additional physics required for this type of interface to form. Recent proof-of-concept calculations performed by the authors have shown that the thick-film steady states are possible in the computational framework of Keeler et al. [59], provided that the flow is body-force driven (for example, a gravity-driven problem; usually important in experiments on the macro scale) as opposed to pressure-driven, see Figure 8. In this formulation, the momentum equation in the liquid phase, (1), is replaced by

$$0 = -\nabla p + \nabla^2 \mathbf{u} + \mathbf{F}, \tag{8}$$

where $\mathbf{F} = (0,F)^T$, and F is a parameter that represents the strength of the force. Further investigations have shown that, in contrast to the pressure-driven problem, the volume of the liquid plays an important role and that a *cusp bifurcation* occurs as the volume is varied, see Figure 8, which is where two fold bifurcations collide and is commonly associated with *catastrophe theory* (see, for example [100]), which was popular in the 1970s and 80s. Interestingly, the solutions shown in Figure 8 are *stable* in the sense that the vertical extent of the thick-film state remains fixed once the system has settled to it. In contrast, thin-film formation which is typically associated with this problem is intrinsically unstable as demonstrated in Keeler et al. [59], where the vertical extent of the thin film increases with time. We remark that in Hayoun et al. [99] the thick films visualised are also time-dependent, and it was remarked that the thickness of this film can be tuned by the pressure; how these observations (which is a pressure-driven problem) and the steady thick-film solution

calculated in Figure 8 (which is a force-driven problem) relate is not known and deserves further study.

Furthermore, different bifurcation structures have been reported before, for example, in the presence of gravity, Chan et al. [62] have shown that the bifurcation curve oscillates around a fixed value of *Ca* (see our yellow curve in Figure 8). However, our preliminary calculations show that as the body force, *F*, is varied (and therefore also *Ca*), the curve appears to persist past for large *Ca*, see red curve in bottom panel of Figure 8. This feature of the bifurcation curve for the force-driven problem, which departs from well-established results in the literature, warrants further investigation, and renewed attention on the force-driven problem is required.

Capillary peeling

In a recent experimental paper, Khodaparast, Boulogne, Poulard, and Stone [101] showed how the ink of a permanent 'Sharpie' marker can be 'peeled' off from a solid substrate as the substrate is slowly lowered into a bath of fluid. The flow field was visualised, and it was hypothesised that one of the key features of the flow that facilitates the peeling process is the existence of a stagnation point at the contact line and a split-injection flow pattern, see Figure 9. This has some potentially interesting applications, including 3D fabrication of objects based on 2D drawing, see Song, Lee, Choe, Kim, Kang, Lee, Choi, Choi, Jeong, Lee, et al. [102].

Figure 7

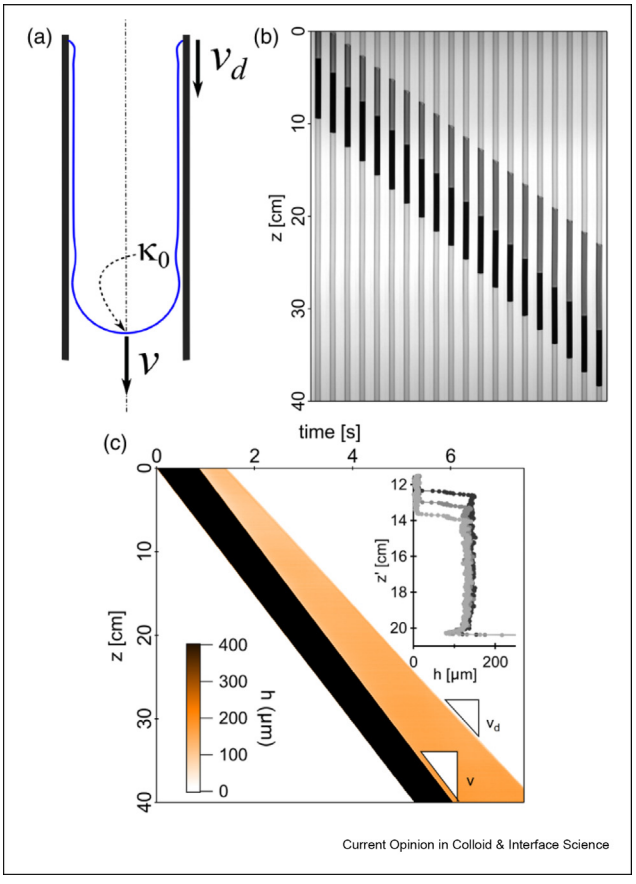

Figure and caption adapted from Hayoun et al. [99] with permission. (**a**): Schematics of the liquid meniscus and matching film. (**b**): A series of 20 snapshots in which a liquid bridge (dark) is forced down a tube (light grey). The medium grey level is the liquid film, and the space–time variations of the film thickness can be measured after calibration of the optical absorption. (**c**) Space–time plot showing film thickness; inset: three successive thickness profiles at 0.5-s time increment, shown in the reference frame of the bridge. As $v_d < v$, the trailing film extends and is seen to do so at constant thickness.

A computational framework based on the NS system is essential to investigate the flow-patterns associated with this phenomenon, which cannot be resolved with a lubrication model. The peeling process was highly dependent on the flow in the liquid phase [101], where inertial effects were prominent. This means that a full resolution of the flow field in the liquid phase, and therefore full computations of the NS system, is required as a starting point to investigate this process. Modelling the detachable layer on the substrate would be challenging, but as an initial avenue of research, understanding the inertial dynamics in the vicinity of the moving contact-line would be of interest. In particular, as seen in Figure 9, there are regions of flow reversal in the liquid phase, and understanding the origin of this, i.e., is it because of surfactants, inertia, or something else, can be determined using the techniques discussed earlier.

3D instability

Highlighting another recent paper, He [32]; He and Nagel [41], remarkable experiments have quantified the 3D structure of the contact-line region observed when a plate is plunged (ACL) or withdrawn (RCL) from a liquid bath, see Figure 10, taken and from He [32]. The formation of the striking 'V-shaped' structure is dynamic, and therefore, a natural test-bed for 3D numerical simulations is to attempt to mimic the phenomenon displayed. In this study, the authors identified two distinct film widths, a thin (Landau–Levich type) and a thick film with increasingly complex coherent structures visible in the system—there may be links to the thick-film structures seen in Hayoun et al. [99] as discussed earlier. We note that this 3D structure was also observed as far back as in Blake and Ruschak [33], where a maximum speed of wetting was hypothesised and the idea that the contact line 'tilts' itself to reduce the speed normal to the substrate was mentioned. This mechanism leads to corners where drops are 'left behind' in the RCL, and it appears to be responsible for the sawtooth pattern/bubbles emerging in the ACL as shown in Vandre et al. [37], see Figure 2. These *corner singularities* have been analysed using lubrication theory in, for example, Snoeijer, Rio, Le Grand and Limat [103] and Limat and Stone [104], but a full 3D computation using the NS system would provide fresh insight into how the structures observed in He [32] can form, in

Figure 8

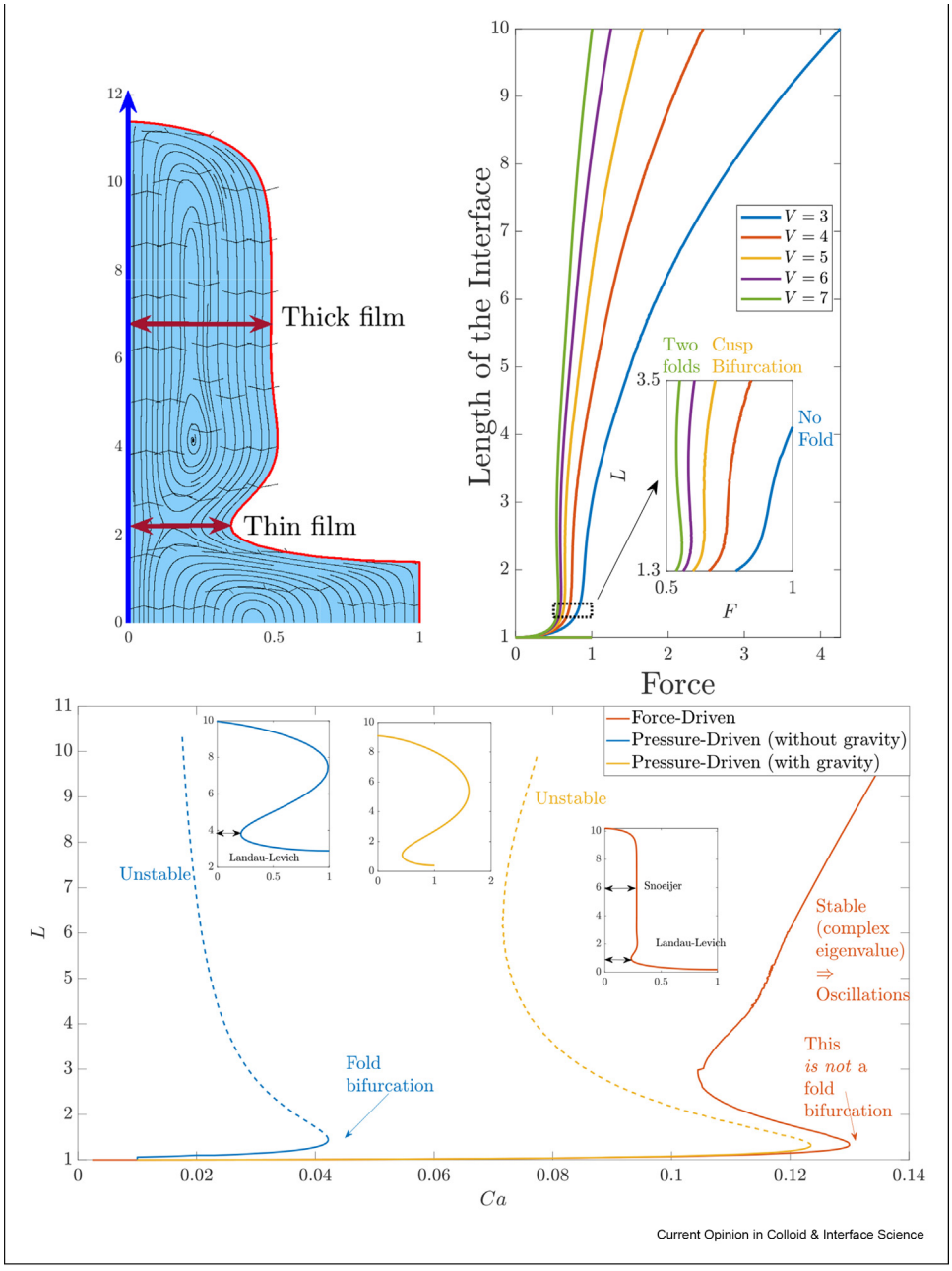

Top left panel: A computed thick-film solution of the Navier–Stokes system with a body force. The two different film thicknesses are indicated with double arrows, and the direction of motion of the solid is also indicated by a single arrow. Top right panel: The bifurcation curves in the (Force, Length of interface) plane for different volumes. The inset shows a zoom of the bifurcation curve showing the cusp bifurcation. Bottom panel: Bifurcation diagram for the pressure-driven (blue curve), pressure-driven with gravity (yellow curve), and force-driven (red curve) with stable/unstable parts indicated by solid/dashed lines, respectively. We note that in this system, the geometry is a plate being withdrawn from an infinite bath (and hence unbounded as $x \to \infty$.).

particular, the calculation of the eigenmodes of any steady state may reveal important information on which structures and patterns become dominant as time progresses.

The sawtooth patterns seen in the ACL (see Figure 2) are also intrinsically 3D, and an open challenge, therefore, is to extend the computational model into a third dimension. In principle, the Finite Element Method (FEM) is conducive to increasing the dimensionality of the problem and in principle can be as simple as changing a 2 to 3 into the code. However, the choice of mesh, as discussed in section A, and mesh-update strategy will be vitally important as the

Figure 9

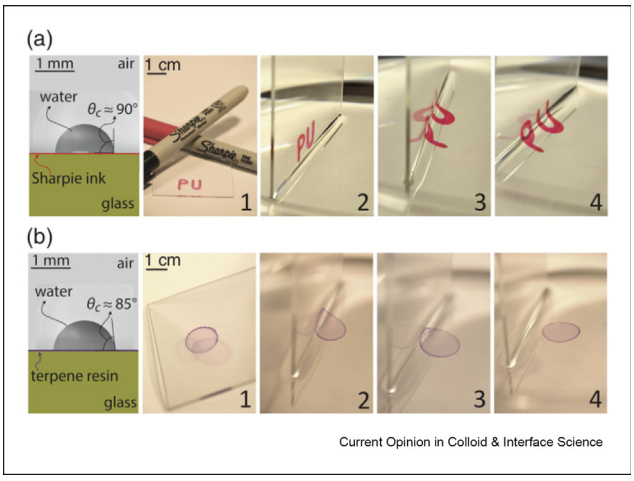

Experimental images of the capillary peeling phenomena. Figure taken from Khodaparast et al. [101] with permission.

Jacobian assembly will scale exponentially with the dimension and computational efficiency will be a key consideration when deciding on the final computational framework.

Thus far, solutions in 3D have been calculated using both diffuse interface models (see, for example [66,97,105,106]) and sharp interface approaches (see, for example [107–109]), but finding eigenmodes and using a dynamical systems approach is yet to be implemented and would represent a significant advance on existing computational capabilities. Calculating 3D steady solutions would be the initial goal, with the intention of determining, from a stability analysis, whether 2D or 3D modes are most unstable, i.e., when is (if at all):

$$Ca_{\mathrm{crit,2D}} = Ca_{\mathrm{crit,3D}}? \tag{9}$$

Answering this question would be of fundamental importance to understanding the dynamic wetting instability; whilst we know that the final unsteady states are often 3D, it is not clear how the system got there—e.g., was it via a 3D linear instability whose growth rate is greater than the 2D modes or by some 3D finite-sized perturbation to a 2D solution? Furthermore, it is not unreasonable to expect further solution branches to exist in the full 3D system, and any time-dependent computational model may be able to visualise these and then, using the dynamical systems approach promoted in Keeler et al. [7], be able to understand the significance of these steady states.

Figure 10

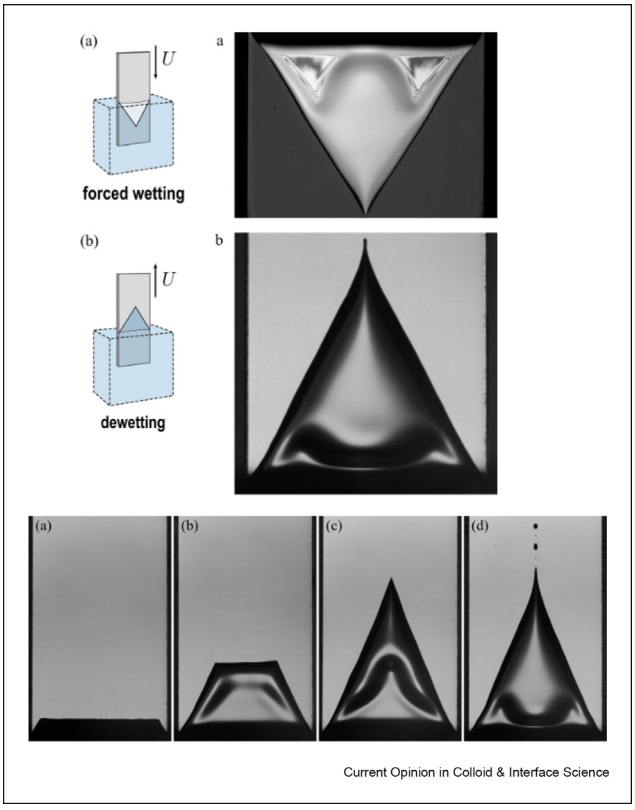

Top panels: Experimental photograph of the three-dimensional structure visible in the advancing contact-line [(a) and (A)] and receding contact-line [(b) and (B)]. Lower panels show the development of a distinctive double-thickness triangular film in the receding contact-line. Figure taken from He [32] with permission.

Final remarks

This is an exciting time in the development of computational models of dynamic wetting, and we are at the cusp of new discoveries in the field. Opening the door to 3D calculations and using the full arsenal of dynamical systems theory has the potential to create new surprising avenues of research. The dynamical systems perspective is a perfect foil for the moving contact-line problem, and the potential to calculate different invariant objects of the system will help us gain valuable insight into how the dynamics of the system evolve in a wide range of physical (de)wetting problems.

Numerical approaches

A range of different numerical approaches have been proposed for capturing free-surface flows described by the conventional equations of fluid mechanics. Arguably the most popular approach is to use the VoF approach, as reviewed in general in Popinet [70] and specifically for wetting problems in Afkhami [15], where interfaces cut through cells and topological changes are 'automatically' handled. In contrast, finite-element approaches that implement an arbitrary Lagrangian Eulerian (ALE)-FEM approach, reviewed recently in Anthony et al. [71], track the interface with nodes to yield high-accuracy

representations of the dynamics there at the expense of flexibility. Notably, both approaches have strong open-source codes that are widely used in the community; e.g., Basilisk (formerly Gerris) for VoF [http://basilisk.fr/src/vof.h] (for ALE-FEM, see further in this article).

We will focus on the ALE-FEM implementation of the NS system, whose application to dynamic-wetting phenomena has been reviewed and described in Sprittles and Shikhmurzaev [110]. In this case, accuracy is relatively easily achieved, and resolving a sharp interface means that including additional physics, such assurface dynamics [42,82,83] or gas kinetic effects [44,111] can also be easily added. Then, the challenge becomes one of 'meshing' the domain with elements in a computationally tractable manner.

In this section, we will focus on the key choices and decisions that have to be made when designing a FEM code to solve a particular dynamic-wetting problem. The first decision to be made is which package to use if at all. One may decide to use a commercial FEM package (such as COMSOL®Multiphysics [112]) and 'throw the kitchen sink' at the problem, but although commercial software offers technical support and is well documented, the advantages of an open-source FEM package is that bespoke physics and equations can more easily be implemented as the source code is easily available and adaptable; the learning curve is steeper, but there is less of ceiling as to what one can achieve. There are many open-source FEM packages that are available; in this article, we note the GOMA package [69], which has been implemented by the Minnesota group and the oomph-lib package [68], (available on https://github.com/oomph-lib/oomph-lib) which has been used in Keeler et al. [7,59].

Once a package has been chosen, there are four main considerations when deciding on what features are required for an individual application: (i) the choice of finite element type, (ii) the mesh-update strategy, (iii) the contact-angle implementation, and (iv) the numerical continuation method. We shall discuss each separately and justify the choices based on new calculations made with the oomph-lib package.

Domain geometry

The fundamental primary consideration is to decide on the shape and structure of the geometric element in the mesh. For a 2D mesh, this means either structured/unstructured quadrilateral or triangular elements, see Figure 11. In principle, a mixture of a structured or unstructured grid can be implemented, but it is significantly easier to choose an element and mesh-type and persist with it throughout the computational domain. Sprittles and Shikhmurzaev [110] implemented a structured triangular mesh, Vandre et al. [80]; Liu et al. [42,81–83]; Charitatos et al. [84]; and Mhatre et al. [85] implemented a structured quadrilateral mesh, and Keeler et al. [7,59] implemented an unstructured triangular mesh. There are advantages and disadvantages to each method. Triangular meshes are more suited for acute contact angles as the a triangle will more naturally 'fit' into the angle required, but for quadrilateral structured meshes, it is easier to identify individual elements that need to be refined so that the accuracy of the solution remains intact; unstructured meshes require an error estimator (in oomph-lib, a ZZ error estimator is used Zienkiewicz and Zhu [113]), which

Figure 11

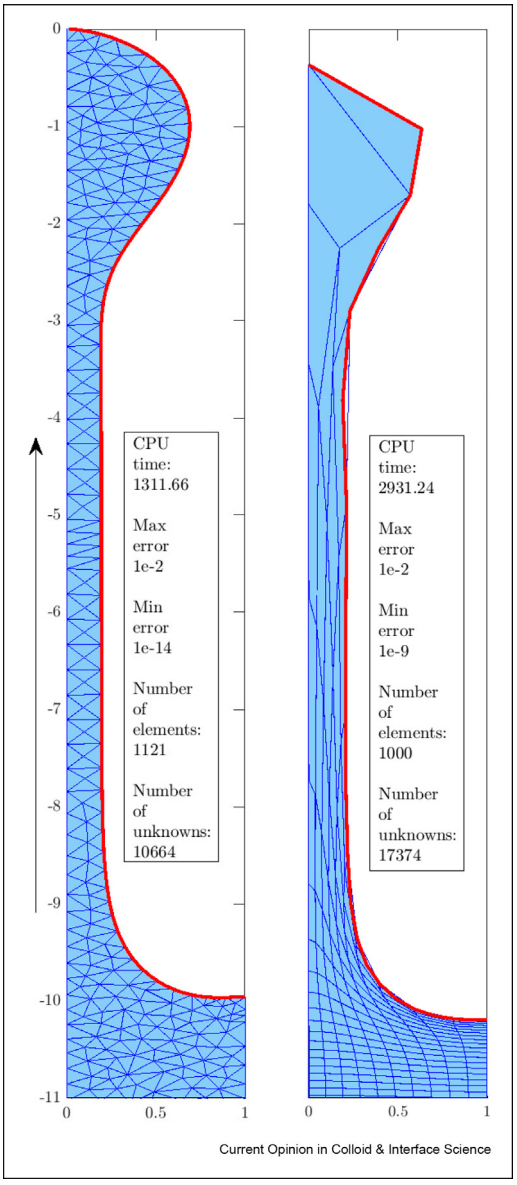

Comparison of the computational solution at the same time-step ($t = 15.0$) with identical error estimates using an unstructured triangular mesh (left figure) and a structured rectangular mesh (right figure) (only a portion of the domain shown). Other parameters are $Ca = 0.4$, $\lambda = 0.1$, $\chi = 0$, $\theta_{cl} = \pi$, and the time-step is $\Delta t = 0$. The initial condition is a flat interface over a fluid at rest with computational area 10.

means there is less control over which elements can be refined/unrefined. As a 'like for like' test, we have performed two time simulations at a value of $Ca > Ca_{\text{crit}}$ for the RCL from a fluid initially at rest with a flat interface on an unstructured triangular grid and a structured rectangular grid using an identical mesh-update strategy (see below). To make the test 'fair', the adaptivity targets for each mesh test was chosen to be identical as well as the frequency at which the mesh was adapted. At the final time-step, the triangular mesh displayed a far more plausible mesh, see left panel of Figure 11, whereas the quadrilateral mesh was very poorly resolved near the contact line, and it is difficult to even call the resulting profile a 'solution'. Furthermore, as can be seen by the stats in the figure, compared to the quadrilateral mesh, the triangular mesh took less than half the CPU-time, used more elements but less nodal unknowns, and hence, demonstrated its superiority over the quadrilateral mesh. Interestingly, the maximum Z2 error for both meshes is of the same magnitude despite the quadrilateral mesh clearly being less resolved; the minimum error is several orders of magnitude less for the triangular mesh, further highlighting the advantages of this domain geometry.

Mesh-update strategy

The secondary consideration in the design is how the position of the interface is updated as the solution curve is traced or as time advances. In the FEM formulation, the kinematic condition, (2), has to be satisfied and determines the position of the interface. The main difficulty is that the shape of the interface is itself an unknown in the problem. In Vandre et al. [80]; Liu et al. [42,81–83]; and Charitatos et al. [84], an *elliptic mesh generation technique* (see, for example Spekreuse [114]) is implemented where the nodal positions of the entire mesh are mapped to a fixed rectangular domain (see Figure 12) via an unknown map, which determines the location of the interface. In Sprittles and Shikhmurzaev [110] and Kamal et al. [64], a *spine method* is used, where a finite number of 'spines' are placed evenly in the mesh where nodes are placed according to a simple rule, and the only unknown is the height of the interface or more generally, the length of the spine. The last mesh-update strategy which we will discuss is the pseudo-solid elastic mesh [115], where all nodal positions are made unknowns in the problem and the mesh moves according to the equations of solid deformations. The advantages of the spine method is that the Jacobian matrix is less sparse, and hence, the linear solve at each Newton step is less costly than the elliptic-mesh and pseudo-elastic methods, but a key disadvantage is that for straight spines, multivalued interfaces are not possible, and the simulations will fail when air entrainment of thin-film development occurs. Even for nonstraight spine meshes, the approach lacks flexibility, and the solution shape needs to be known *a priori* before constructing the mesh. The elastic mesh is the most flexible method when simulating the time-dependent problem as it the shape of the mesh that evolves naturally as a response to the shape of the interface and does not require any *a priori* mesh design.

Contact-angle implementation

Sprittles and Shikhmurzaev [110] describes three possible implementations for the contact angle, each of which, in the limit of shrinking grid size, gives the same result. In the first two approaches, for (A–a) the contact angle is imposed as a 'natural condition' with one component of the momentum equation 'dropped', whereas for (A-b) the contact angle is imposed as an 'essential condition' with two components of the momentum equation 'dropped'. However, in approach B of Sprittles and Shikhmurzaev [110], the angle is implemented as a 'natural condition', and an extra set of unknowns are added to the moving wall, which act as Lagrange multipliers to the no-penetration condition and ensure that curved walls can be treated as easily as flat ones. The key difference in this approach is that all NS equations can be implemented at the contact line (so that on curved surfaces no rotation of momentum equations is required in order to establish which one should be 'dropped' to enforce impermeability). As shown in Sprittles and Shikhmurzaev [110], for a given mesh, approach B is more accurate, and this has consequently been implemented in the recent work of Keeler et al. [7,59].

Figure 12

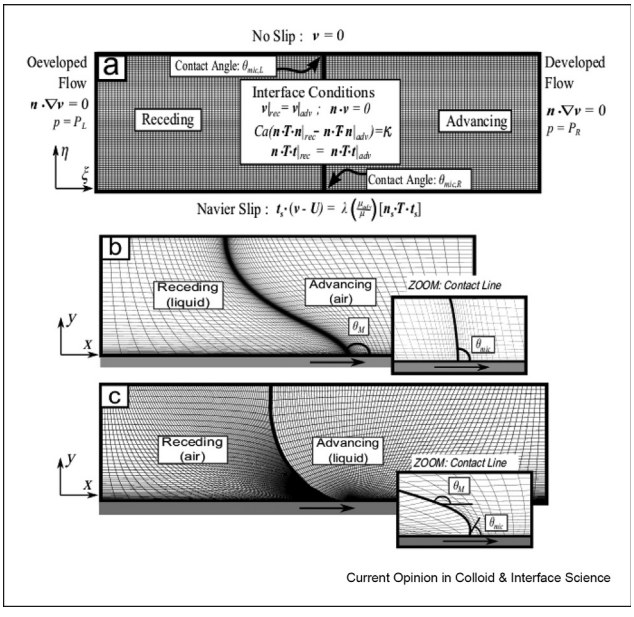

Taken from Vandre [46]. The top panel is the computational mesh that is fixed and mapped to the physical domain in panels b and c by solving a set of nonlinear equations.

Continuation procedure

When calculating the full steady solution space, i.e., the stable and unstable solution branches, it is natural to start at a very small *Ca* so that the interface has small curvature, and hence, a good initial guess for the nonlinear solver is simply a flat interface. Presuming that a converged solution is found for a suitably small *Ca*, any naïve attempt to incrementally increase the value of *Ca* is doomed to fail as eventually the system will encounter Ca_{crit} and it will be impossible to increase *Ca* any further as no steady state exists. To traverse the fold bifurcation and start calculating the unstable branch of solutions, a user has to let *Ca* come as part of the solution and be determined by an additional constraint. The most general approach is to use a pseudo-arclength constraint that ensures the next solution is a fixed distance further along the bifurcation curve from the current solution (see, for example [116]). However, an easier approach is to use a system measure as a continuation parameter and a new constraint that controls this value that implicitly determines the value of *Ca*. For example, the overall length of the interface increases monotonically as the solution curve is traced around the fold, and therefore, by controlling the length of the interface and letting *Ca* be implicitly determined by this constraint, the fold bifurcation can be traced out and the unstable branch of solutions can be found. This approach was used in Keeler et al. [7,59].

Finally, we note that, for this dynamic-wetting problem, a direct comparison between different FEM frameworks, for example between oomph-lib and GOMA, and different VoF frameworks would be of considerable interest for researchers when making a choice of what framework to implement (similar to Hysing, Turek, Kuzmin, Parolini, Burman, Ganesan, and Tobiska [117] for the rising bubble problem). Such a comparison is beyond the scope of this review article, but we propose the calculation in Figure 11 as suitable benchmark calculation that can be used to compare with other frameworks.

CRediT authorship contribution statement

J. S. Keeler: Writing - Original draft preparation. **J. E. Sprittles:** Writing - Original draft preparation.

Declaration of competing interest

The authors declare the following financial interests/personal relationships which may be considered as potential competing interests:Jack Keeler reports financial support was provided by Leverhulme Trust.

Data availability

Data will be made available on request.

Acknowledgments

J.S.K gratefully acknowledges funding by the Leverhulme Trust, ECF-2021-017. J.E.S. gratefully acknowledges EPSRC under grants EP/W031426/1, EP/S022848/1 and EP/P031684/1 For the purpose of open access, the author has applied a CC BY public copyright licence to any Author Accepted Manuscript version arising from this submission.

References

Papers of particular interest, published within the period of review, have been highlighted as:

* of special interest
** of outstanding interest

1. Stone HA, Stroock AD, Ajdari A: **Engineering flows in small devices: microfluidics toward a lab-on-a-chip**. *Annu Rev Fluid Mech* 2004, **36**:381–411.

2. Weinstein SJ, Ruschak KJ: **Coating flows**. *Annu Rev Fluid Mech* 2004, **36**:29–53.

3. Gerritsen MG, Durlofsky LG: **Modelling fluid flow in oil reservoirs**. *Annu Rev Fluid Mech* 2005, **37**:211–238.

4. Papierowska E, Szporak-Wasilewska S, Szewińska J, Szatyłowicz J, Debaene G, Utratna M: **Contact angle measurements and water drop behavior on leaf surface for several deciduous shrub and tree species from a temperate zone**. *Trees* 2018, **32**:1253–1266.

5. Beatty SM, Smith JE: **Fractional wettability and contact angle dynamics in burned water repellent soils**. *J Hydrol* 2010, **391**:97–108.

6. Barthlott W, Mail M, Neinhuis C: **Superhydrophobic hierarchically structured surfaces in biology: evolution, structural principles and biomimetic applications**. *Phil. Trans. R. Soc. A* 2016, **374**, 20160191.

7. ** Keeler JS, Lockerby DA, Kumar S, Sprittles JE: **Stability and bifurcation of dynamic contact lines in two dimensions**. *J Fluid Mech* 2022, **945**:A34.
This paper contains all of the detailed analysis and numerical simulations that have been discussed in this review, with regards to the dynamical systems interpretation of the moving contact-line.

8. Miyamoto K, Katagiri Y: **Curtain coating**. *Liquid Film Coating: Scientific principles and their technological implications* 1997:463–494.

9. Blake TD, Dobson R, Batts GN, Harrison WJ: *Coating processes*. US patent; 1995, 5391401.

10. Blake TD, Dobson RA, Ruschak KJ: **Wetting at high capillary numbers**. *J Colloid Interface Sci* 2004, **279**:198–205.

11. Afkhami S, Gambaryan-Roisman T, Pismen LM: **Challenges in nanoscale physics of wetting phenomomen**. *Eur Phys J Spec Top* 2020, **229**:1735–1738.

12. Semenov S, Starov VM, Velarde MG, Rubio RG: **Droplets evaporation: problems and solutions**. *Eur Phys J Spec Top* 2011, **197**:265–278.

13. Andreotti B, Snoeijer JH: **Statics and dynamics of soft wetting**. *Annu Rev Fluid Mech* 2020, **52**:285–308.

14. Semenov S, Starov VM, Velarde MG, Rubio RG: **Droplets evaporation: problems and solutions**. *Eur Phys J Spec Top* 2011, **197**:265–278.

15. Afkhami S: **Challenges of numerical simulation of dynamic wetting phenomena: a review**. *Curr. Op. J. Coll. Inter. Sci.* 2022, **57**:1523.

16. Fullana T, Zaleski S, Popinet S: **Dynamic wetting failure in curtain coating by the volume-of-fluid method: volume-of-fluid simulations on quadtree meshes**. *Eur Phys J Spec Top* 2020, **229**:1923–1934.

17. Christodoulou KN, Scriven LE: **Finding leading modes of a viscous free surface flow: an asymmetric generalized eigenproblem**. *J Sci Comput* 1988, **3**:355–406.

18. Severtson YC, Aidun CK: **Stability of two-layer stratified flow in inclined channels: applications to air entrainment in coating systems**. *J Fluid Mech* 1996, **312**:173–200.

19. Eckhardt B, Faisst H, Schmiegel A, Schneider TM: **Dynamical systems and the transition to turbulence in linearly stable shear flows**. *Phil Trans Roy Soc Lond* 2008, **366**:1297–1315.

20. Gallino G, Schneider TM, Gallaire F: **Edge states control droplet breakup in subcritical extensional flows**. *Phys. Rev. Fluids* 2018, **3**, 073603.

21. Gaillard A, Keeler JS, Thompson A,J, Hazel AH, Juel A: **Life and fate of a bubble in a constricted hele-shaw channel**. *J Fluid Mech* 2020, **122**:12.

22. Keeler JS, Thompson AB, Lemoult G, Juel A, Hazel AL: **The influence of invariant solutions on the transient behaviour of an air bubble in a hele-shaw channel**. *Proc Roy Soc Lond A* 2019, **879**:1–27.

23. Poincaré H. *Les méthodes nouvelles de la mécanique céleste*, **3**. imprimeurs-libraires: Gauthier-Villars et fils; 1899.

24. Kolmogorov A: **Théorie générale des systèmes dynamiques de la mécanique classique**. *Séminaire Janet. Mécanique analytique et mécanique céleste* 1957, **1**:1–20.

25. Kuznetsov YA: *Elements of applied bifurcation theory*. 3rd ed. Springer-Verlag; 1998.

26. Brunton SL, Proctor JL, Kutz JN: **Discovering governing equations from data by sparse identification of nonlinear dynamical systems**. *Proc Natl Acad Sci USA* 2016, **113**: 3932–3937.

27. Brunton SL, Kutz JN: *Data-driven science and engineering: machine learning, dynamical systems, and control*. Cambridge University Press; 2022.

28. Kutz JN: **Deep learning in fluid dynamics**. *J Fluid Mech* 2017, **814**:1–4.

29. Heroux M, Bartlett R, Howle V, Hoekstra R, Hu J, Kolda T, Lehoucq R, Long K, Pawlowski R, Phipps E, Salinger A, Thornquist H, Tuminaro R, Willenbring J, Williams A: *An overview of Trilinos*. Sandia National Laboratories; 2003. Technical Report. SAND2003-2927.

30. Schmid PJ: **Dynamic mode decomposition of numerical and experimental data**. *J Fluid Mech* 2010, **656**:5–28.

31. Page J, Kerswell RR: **Koopman mode expansions between simple invariant solutions**. *J Fluid Mech* 2019, **879**:1–27.

32. * He M: **Long-time evolution of interfacial structure of partial wetting**. *Phys. Rev. Fluids* 2020, **5**, 114001.
This paper has some superb experimental imagery and analysis on the 3D 'vee-shaped' pattern in both the receding and advancing contact-line.

33. Blake TD, Ruschak KJ: **A maximum speed of wetting**. *Nature* 1979, **282**:489–491.

34. Simpkins PG, Kuck VJ: **Air entrapment in coatings by way of a tip-streaming meniscus**. *Nature* 2000, **403**:641–643.

35. Duez C, Ybert C, Clanet C, Bocquet L: **Making a splash with water repellency**. *Nat Phys* 2007, **3**:180–183.

36. Pack M, Kaneelil P, Kim H, Sun Y: **Contact line instability caused by air rim formation under nonsplashing droplets**. *Langmuir* 2018, **34**:4962–4969.

37. Vandre E, Carvalho MS, Kumar S: **Characteristics of air entrainment during dynamic wetting failure along a planar substrate**. *J Fluid Mech* 2014, **747**:119–140.

38. Snoeijer JH, Delon G, Andreotti B, Fermigier M: **Avoided critical behavior in dynamically forced wetting**. *Phys Rev Lett* 2006, **96**.

39. Snoeijer JH, Ziegler J, Andreotti B, Fermigier M, Eggers J: **Thick films of viscous fluid coating a plate withdrawn from a liquid reservoir**. *Phys Rev Lett* 2008, **100**, 244502.

40. Podgorski T, Flesselles JM, Limat L: **Corners, cusps, and pearls in running drops**. *Phys Rev Lett* 2001, **87**, 036102.

41. He M, Nagel SR: **Characteristic interfacial structure behind a rapidly moving contact line**. *Phys Rev Lett* 2019, **122**, 018001.

42. Liu CY, Carvalho MS, Kumar S: **Dynamic wetting failure in curtain coating: comparison of model predictions and experimental observations**. *Chem Eng Sci* 2019, **195**:74–82.

43. Vandre E, Carvalho MS, Kumar S: **Delaying the onset of dynamic wetting failure through meniscus confinement**. *J Fluid Mech* 2012, **707**:496–520.

44. Sprittles JE: **Kinetic effects in dynamic wetting**. *Phys Rev Lett* 2017, **118**, 114502.

45. Snoeijer JH, Andreotti B, Delon G, Fermigier M: **Relaxation of a dewetting contact line. part 1. a full-scale hydrodynamic calculation**. *J Fluid Mech* 2007, **579**:63–83.

46. Vandre E: *Onset of dynamic wetting failure: the mechanics of high-speed fluid displacement*. USA: Ph.D. thesis. University of Minnesota; 2013.

47. Hocking LM: **The spreading of a thin drop by gravity and capillarity**. *Q J Mech Appl Math* 1983, **36**:55–69.

48. Cox RG: **The dynamics of the spreading of liquids on a solid surface. part 1. viscous flow**. *J Fluid Mech* 1986, **168**:169–194.

49. Oron A, Davis HS, Bankoff GS: **Long-scale evolution of thin liquid films**. *Rev Mod Phys* 1997, **69**:931.

50. Blake TD: **The physics of moving wetting lines**. *J Colloid Interface Sci* 2006, **299**:1–13.

51. Blake TD, Haynes JM: **Kinetics of liquid/liquid displacement**. *J Colloid Interface Sci* 1967, **14**:421–423.

52. Blake TD: **Dynamic contact angles and wetting kinetics**. In *Wettability*. Edited by Berg JC; 1993:251–309.

53. Fernádez-Tolendano JC, Blake TD, De Coninck J: **Moving contact lines and Langevin formalism**. *J Colloid Interface Sci* 2020, **562**:287–292.

54. Fernádez-Tolendano JC, Blake TD, De Coninck J: **Contact-line fluctuations and dynamic wetting**. *J Colloid Interface Sci* 2019, **540**:322–329.

55. Fernández-Toledano JC, Blake TD, Coninck JD: **The hidden microscopic life of the moving contact line of a waterlike liquid**. *Phys. Rev. Fluids* 2020, **5**, 104004.

56. Shikhmurzaev YD: *Capillary flows with forming interfaces*. CRC Press; 2007.

57. Karim AM, Suszynski WJ: **Physics of dynamic contact line: hydrodynamics theory versus molecular kinetic theory, challenges of numerical simulation of dynamic wetting phenomena: a review**. *Fluid* 2022, **7**:318.

58. Bonn D, Eggers J, Indekeu J, Meunier J, Rolley E: **Wetting and spreading**. *Rev Mod Phys* 2009, **81**:739.

59. Keeler JS, Blake TD, Lockerby DA, Sprittles JE: **Putting the micro into the macro: using a molecularly-augmented hydrodynamic model to investigate the flow instability of a liquid nano plug**. *J Fluid Mech* 2022, **953**:A17.

60. Eggers J: **Towards a description of contact line motion at higher capillary numbers**. *Phys Fluids* 2004, **16**:3491–3494.

61. Eggers J: **Existence of receding and advancing contact lines**. *Phys Fluids* 2005, **17**.

62. Chan TS, Snoeijer JH, Eggers J: **Theory of the forced wetting transition**. *Phys Fluids* 2012, **24**.

63. Snoeijer JH, Andreotti B: **Moving contact lines: scales, regimes, and dynamical transitions**. *Annu Rev Fluid Mech* 2013, **45**:269–292.

64. Kamal C, Sprittles JE, Snoeijer JH, Eggers J: **Dynamic drying transition via free-surface cusps**. *J Fluid Mech* 2019, **858**.

65. Chan TS, Kamal C, Snoeijer JH, Sprittles JE, Eggers J: **Cox–voinov theory with slip**. *J Fluid Mech* 2020, **900**:A8.

66. Jacqmin D: **Onset of wetting failure in liquid–liquid systems**. *J Fluid Mech* 2004, **517**.

67. Sbragaglia M, Sugiyama K, Biferale L: **Wetting failure and contact line dynamics in a Couette flow**. *J Fluid Mech* 2008, **614**:471–493.

68. Heil M, Hazel AL: **oomph-lib–an object-oriented multi-physics finite-element library**. In *Fluid-structure interaction*. Springer; 2006:19–49.

69. Schunk PR, Rao RR, Chen KS, Labreche DA, Sun ACT, Hopkins MM, Moffat HK, Roach RA, Hopkins PL, Notz PK, *et al.*: *Goma 6.0-a full-Newton finite element program for free and moving boundary problems with coupled fluid/solid momentum, energy, mass, and chemical species transport: user's guide*. Albuquerque, NM (United States); 3M: Sandia National Lab.(SNL-NM); 2013. Technical Report.

70. Popinet S: **Numerical models of surface tension**. *Annu Rev Fluid Mech* 2018, **50**:49–75.

71. Anthony CR, Wee H, Garg V, Thete SS, Kamat PM, Wagoner BW, Wilkes ED, Notz PK, Chen AU, Suryo R, Sambath K, Panditaratne JC, Liao YC, Basaran OA: **Sharp interface methods for simulation and analysis of free surface flows with singularities: breakup and coalescence**. *Annu Rev Fluid Mech* 2023, **55**.

72. Li XS: **An overview of superlu: algorithms, implementation, and user interface**. *ACM Trans Math Software* 2005, **31**: 302–325.

73. Huh C, Scriven LE: **Hydrodynamic model of steady movement of a solid/liquid/fluid contact line**. *J Colloid Interface Sci* 1971, **35**:85–101.

74. Dussan V: **The moving contact line: the slip boundary condition**. *J Fluid Mech* 1976, **77**:665–684.

75. Dussan VEB: **On the spreading of liquids on solid surfaces: static and dynamic contact lines**. *Annu Rev Fluid Mech* 1979, **11**:371–400.

76. Voinov OV: **Hydrodynamics of wetting**. *Fluid Dynam* 1976, **11**: 714–721.

77. Eggers J: **Hydrodynamic theory of forced dewetting**. *Phys Rev Lett* 2004, **96**.

78. Chan TS, Srivastava S, Marchand A, Andreotti B, Biferale L, Toschi F, Snoeijer JH: **Hydrodynamics of air entrainment by moving contact lines**. *Phys Fluids* 2013, **25**, 074105.

79. Eggers J: **Air entrainment through free-surface cusps**. *Phys Rev Lett* 2001, **86**:4290.

80. Vandre E, Carvalho MS, Kumar S: **On the mechanism of wetting failure during fluid displacement along a moving substrate**. *Phys Fluids* 2013, **25**.

81. Liu CY, Vandre E, Carvalho MS, Kumar S: **Dynamic wetting failure and hydrodynamic assist in curtain coating**. *J Fluid Mech* 2016, **808**:290–315.

82. Liu CY, Vandre E, Carvalho MS, Kumar S: **Dynamic wetting failure in surfactant solutions**. *J Fluid Mech* 2016, **789**:285–309.

83. Liu CY, Carvalho MS, Kumar S: **Mechanisms of dynamic wetting failure in the presence of soluble surfactants**. *J Fluid Mech* 2017, **825**:677–703.

84. Charitatos V, Suszynski WJ, Carvalho MS, Kumar S: **Dynamic wetting failure in shear-thinning and shear-thickening liquids**. *J Fluid Mech* 2020, **892**.

85. Mhatre VN, Carvalho MS, Kumar S: **Delaying dynamic wetting failure using thermal marangoni flow**. *Phys. Rev. Fluids* 2022, **7**, 124002.

86. Stay MS, Barocas VH: **Coupled lubrication and Stokes flow finite elements**. *Int J Numer Methods Fluid* 2003, **42**:129–146.

87. Holm DD, Marsden JE, Ratiu T, Weinstein A: **Nonlinear stability of fluid and plasma equilibria**. *Phys Rep* 1985, **123**:1–116.

88. Drazin PG: *Nonlinear systems*. Cambridge University Press; 1992.

89. Kumar S: *Nonmodal amplification of disturbances in channel flows of viscoelastic fluids*. 2023.

90. Jovanović MR, Kumar S: **Nonmodal amplification of stochastic disturbances in strongly elastic channel flows**. *JNNFN* 2011, **166**:755–778.

91. Lieu BK, Jovanović MR, Kumar S: **Worst-case amplification of disturbances in inertialess Couette flow of viscoelastic fluids**. *J Fluid Mech* 2013, **723**:232–263.

92. Garnaud X, Lesshafft L, Schmid P, Huerre P: **Modal and transient dynamics of jet flows**. *Phys Fluids* 2013, **25**, 044103.

93. Blackburn HM, Barkley D, Sherwin SJ: **Convective instability and transient growth in flow over a backward-facing step**. *J Fluid Mech* 2008, **603**:271–304.

94. Drazin PG, Reid WH: *Hydrodynamic stability*. Cambridge University Press; 2004.

95. Sprittles JE, Shikhmurzaev YD: **Finite element simulation of dynamic wetting flows as an interface formation process**. *J Comp Physiol* 2013, **233**:34–65.

96. Landau L, Levich B: **Dragging of a liquid by a moving plate**. In *Dynamics of curved fronts*. Elsevier; 1988:141–153.

97. Wu M, Hu L, Su R, Fu X: **Wetting transition of the confined receding meniscus with tailing bead formation**. *Colloids Surf A Physicochem Eng Asp* 2021, **628**, 127316.

98. Hayoun P: **Partial wetting of thin liquid films in polymer tubes**. *Ph.D. thesis. l'Université Pierre et Marie Currie* 2016.

99. * Hayoun P, Letailleur A, Teisseire J, Lequeux F, Verneuil E, Barthe E: **Triple line destabilization: tuning film thickness through meniscus curvature**. *Phys. Rev. Fluids* 2022, **7**, 064002.

This paper has experimental imagery and lubrication analysis on the thick-film solutions.

100. Zeeman EC: **Catastrophe theory**. *Sci Am* 1976, **234**:65–83.

101. * Khodaparast S, Boulogne F, Poulard C, Stone HA: **Water-based peeling of thin hydrophobic films**. *Phys Rev Lett* 2017, **119**, 154502.

This paper is highlighted as an interesting application of flow transitions in a moving contact-line problem and how the dynamical systems approach may be applied to gain further insight into the flow patterns visible in the capillary peeling phenomena.

102. Song SW, Lee S, Choe JK, Kim NH, Kang J, Lee AC, Choi Y, Choi A, Jeong Y, Lee W, *et al.*: **Direct 2d-to-3d transformation of pen drawings**. *Sci Adv* 2021, **7**, eabf3804.

103. Snoeijer JH, Rio E, Le Grand N, Limat L: **Self-similar flow and contact line geometry at the rear of cornered drops**. *Phys Fluids* 2005, **17**, 072101.

104. Limat L, Stone HA: **Three-dimensional lubrication model of a contact line corner singularity**. *Europhys Lett* 2004, **65**:365.

105. Li HL, Liu HR, Ding H: **A fully 3d simulation of fluid-structure interaction with dynamic wetting and contact angle hysteresis**. *J Comp Physiol* 2020, **420**, 109709.

106. Zhou C, Yue P, Feng JJ, Ollivier-Gooch CF, Hu HH: **3d phase-field simulations of interfacial dynamics in newtonian and viscoelastic fluids**. *J Comp Physiol* 2010, **229**:498–511.

107. Dodds S, Carvalho MS, Kumar S: **The dynamics of three-dimensional liquid bridges with pinned and moving contact lines**. *J Fluid Mech* 2012, **707**.

108. Campana DM, Ubal S, Giavedoni MD, Saita FA, Carvalho MS: **Three dimensional flow of liquid transfer between a cavity and a moving roll**. *Chem Eng Sci* 2016, **149**:169–180.

109. Fraggedakis D, Papaioannou J, Dimakopoulos Y, Tsamopoulos J: **Discretization of three-dimensional free surface flows and moving boundary problems via elliptic grid methods based on variational principles**. *J Comp Physiol* 2017, **344**:127–150.

110. Sprittles JE, Shikhmurzaev YD: **Finite element framework for describing dynamic wetting phenomena**. *Int J Numer Methods Fluid* 2012, **68**:1257–1298.

111. Chubynsky MV, Belousov KI, Lockerby DA, Sprittles JE: **Bouncing off the walls: the influence of gas-kinetic and van**

der waals effects in drop impact. *Phys Rev Lett* 2020, **124**, 084501.

112. Multiphysics C: *Introduction to comsol multiphysics®*. Burlington, MA: COMSOL Multiphysics; 1998. . Accessed 9 February 2018.

113. Zienkiewicz OC, Zhu JZ: **The superconvergent patch recovery and a posteriori error estimates. Part 1: the recovery technique**. *Int J Numer Methods Eng* 1992, **33**:1331–1364.

114. Spekreuse SP: **Elliptic grid generation based on laplace equations and algebraic transformations**. *J Comp Physiol* 1995, **118**:38–61.

115. Sackinger PA, Schunk PR, Rao RR: **A newton–raphson pseudo-solid domain mapping technique for free and moving boundary problems: a finite element implementation**. *J Comp Physiol* 1996, **125**:83–103.

116. Doedel EJ: **Lecture notes on numerical analysis of nonlinear equations**. In *Numerical continuation methods for dynamical systems*. Springer; 2007:1–49.

117. Hysing S, Turek S, Kuzmin D, Parolini N, Burman E, Ganesan S, Tobiska L: **Quantitative benchmark computations of two-dimensional bubble dynamics**. *Int J Numer Methods Fluid* 2009, **60**:1259–1288.